International Journal of Mechanical Sciences 157–158 (2019) 849–857

Contents lists available at ScienceDirect

International Journal of Mechanical Sciences

journal homepage: www.elsevier.com/locate/ijmecsci

Design of dielectric elastomer actuators for vibration control at high frequencies

Itsuro Kajiwara[a,*], Shigeki Kitabatake[a], Naoki Hosoya[b], Shingo Maeda[b]

[a] Division of Human Mechanical Systems and Design, Hokkaido University, N13, W8, Kita-ku, Sapporo 060-8628, Japan
[b] Department of Engineering Science and Mechanics, Shibaura Institute of Technology, 3-7-5 Toyosu, Koto-ku, Tokyo 135-8548, Japan

ARTICLE INFO

Keywords:
Dielectric elastomer actuator
Smart structure
Vibration control
Modal analysis
Modal strain energy

ABSTRACT

This study evaluates the basic characteristics of smart structures composed of dielectric elastomer actuators (DEAs) to suppress vibrations. A DEA, which is a lightweight, flexible polymer that can induce high deformations, should realize next-generation actuators. Additionally, DEA can achieve vibration control of structures with complex shapes or curved surfaces. Herein the performance and efficacy of DEAs are evaluated as an actuator for vibration control at high frequencies. First, the appropriate DEA structure is considered. Second, the control system for the smart structure using the DEA is modeled and designed as an actuator. Third, a method to determine DEA's optimum arrangement and shape is discussed by focusing on the structure's strain energy. Finally, a control simulation and a control experiment validate the vibration suppression effects and the efficacy of the DEA.

1. Introduction

A dielectric elastomer actuator (DEA) is a lightweight flexible polymer actuator. In recent years, DEAs have received much attention due to their potential as next-generation actuators [1–19] and as energy-saving devices because they have low manufacturing costs and can efficiently convert electrical energy into mechanical energy (theoretical efficiency 80–90%) [8]. Because DEAs realize flexible and quiet movements that imitate living bodies' functions, it can be shaped similar to rubber. These features permit a high degree of design freedom. Unlike traditional actuators using motors or similar devices, DEAs can achieve a soft and natural touch because it is a polymer.

A dielectric elastomer has a capacitor structure where a thin rubber-like polymeric dielectric film is sandwiched between flexible and expandable electrodes. Applying a voltage between the electrodes creates an electrostatic attractive force, causing the polymeric film to contract in the thickness direction and expand in the film plane direction [1–5]. One application of DEAs is spherical omnidirectional loudspeakers [6] and balloon speakers [7]. Because the main material for dielectric elastomer-based loudspeakers is a polymer, these loudspeakers are lighter than conventional coil- and magnet-based loudspeakers, easier to shape, and respond quickly to electric stimulations [1,6,8]. Dielectric elastomers are used for actuators to directly convert electric energy into mechanical energy. Research has been conducted on a broad range of other applications, including micropumps [9], electricity generating devices [10], and acoustic loudspeakers [11–14].

Heydt et al. studied a mechanism utilizing the bending vibration of pores on a film [11] and sound radiation properties [12]. Sugimoto et al. examined a mechanism involving the bending vibrations of semicylinders [13] and explored loudspeakers using a push-pull mechanism [14]. In addition, the applicability and practicality of DEAs has been enhanced by improving the electromechanical behavior of DEAs [15], reducing the operation voltage [16], integrating a soft ionogel and DEA-based optical devices [17], applying DEAs to soft robotic fingers [18], and a deformable motor [19].

Modeling of DEAs and active vibration control using DEAs as actuators have been investigated to effectively suppress vibrations. Papaspiridis and Antoniadis electrically and mechanically modeled DEAs and conducted active vibration control [20]. Using a basic control scheme, they demonstrated that the DEA can signficantly suppress the vibrations induced by an external force. Sarban et al. reviewed the fabrication, characterization, and active vibration isolation performance of a core-free rolled tubular DEA [21]. Later, Sarban and Jones investigated active vibration isolation with time-varying loads using a feedforward adaptive control approach [22]. Berselli et al. employed a hyperviscoelastic model of a rectangular constant-force actuator as an engineering tool to design and control actuators [23]. Additionally, Karsten et al. used the least mean squares parametric estimation method to

* Corresponding author.
E-mail addresses: ikajiwara@eng.hokudai.ac.jp (I. Kajiwara), s-kitabatake@frontier.hokudai.ac.jp (S. Kitabatake), hosoya@sic.shibaura-it.ac.jp (N. Hosoya), maeshin@shibaura-it.ac.jp (S. Maeda).

https://doi.org/10.1016/j.ijmecsci.2019.05.019
Received 24 August 2018; Received in revised form 25 April 2019; Accepted 13 May 2019
Available online 17 May 2019

dynamically model DEAs and to design a control algorithm for vibration suppression [24]. Although these previous studies employ DEAs, the design method of DEAs to enhance the vibration control performance at high frequencies and their experimental validations have yet to be reported.

Lead zirconate titanates (PZTs) are traditionally found in vibration control actuators using smart structure technologies, where PZTs are attached on the structural surface [25–28]. Adaptive control of a smart structure using PZT is also examined by applying SPSA algorithm [29]. However, installing PZTs on a curved surface is difficult due to the rigidity of the structure. If a method employing a dielectric elastomer actuator for vibration control can be established, vibrations of complicated structures such as those with curved surfaces can be suppressed effectively. Applications of flexible DEA actuators include deformable motors [19], speakers [6,7,11–14], soft robots [30], and soft grippers [31]. By taking advantage of the generation functions of movements and vibrations, DEAs can also act as an actuator for vibration control in various mechanical systems with curved surfaces, including aircraft, flexible films, and building structures. Hence, DEA actuators have potential in diverse applications.

This study employs a DEA to establish a smart structure and examines the structure for effective vibration control. This paper presents the manufacturing method, evaluates the characteristics of the prepared DEA, and determines an effective DEA structure for a vibration control actuator. Additionally, processes to model and design a control system for smart structures employing DEAs are presented. Then a method to determine the optimum arrangement and shape is discussed with an emphasis on the structure's strain energy. Next, a control simulation and experiment are carried out using H_∞ control strategy [29,32]. Finally, the simulation and experiment validate the vibration suppression effects and the efficacy of the vibration control method using the proposed DEA.

2. DEA

2.1. Activation mechanism

Fig. 1 shows the volume changing mechanism of the DEA. When stretchable electrodes are attached to both sides of the elastomer and a voltage is applied, the Maxwell stress acts in the elastomer's thickness direction. This extends the elastomer, which is a non-compressive material, in the in-plane direction. Perline et al. have reported that Maxwell stress (P) acting on an elastomer is expressed as

$$P = \varepsilon_0 \varepsilon_r \left(\frac{V}{d} \right)^2 \tag{1}$$

Here, ε_0 and ε_r represent the vacuum permittivity and the relative permittivity, respectively. Meanwhile, V and d denote the applied voltage and the distance between two electrodes, respectively. This equation shows that the stress increases in proportion to the square of the applied voltage and the inverse of the distance between the electrodes. Typical elastomers are comprised of acrylic-based or silicone-based materials. Elastomers made from such materials show the highest deformation (maximum strain: > 200%) among electrically active polymers [8]. To validate the efficacy as an actuator, we prepared acrylic-based DEA and attached it to the structure in an excitation experiment to evaluate dynamic characteristics. Using these processes, a vibration control method is examined based on feedback control.

2.2. Fabrication

Acrylic-based elastomers and carbon nanotubes (CNT) are used for the elastomer and the electrode parts of the DEA, respectively. Pre-stretching thins the elastomer and contributes to the increased dielectric breakdown strength. Here the 80 × 80 mm elastomer sheet is expanded to a 320 × 320 mm sheet. After pre-stretching, the elastomer is attached to a fixing frame to maintain the pre-stretched state.

Fig. 2 depicts the process of applying CNT to the elastomer using a circular electrode to create a one-layer DEA as an example. Process A attaches a piece of the pattern sheet cut into the intended shape and applies a CNT to the sheet (Fig. 2(a)). Herein a removable pattern sheet with a CNT is used. This pattern sheet works as the flexible electrode part that can be removed once attached to the elastomer. Process B removes the pattern sheet to create a wire with a CNT (Fig. 2(b)). Process C reverses the fixing frame and applies a CNT to the back surface of the elastomer similar to Process B (Fig. 2(c)). Finally, Process D sandwiches the elastomer unit between the flexible CNT electrodes (Fig. 2(d)). Keeping the pre-stretched state, the elastomer unit with the CNT electrodes is attached to a structure to fabricate an actuator for vibration control and then cut from the base elastomer. Here, the unit layer is the number of elastomers.

3. DEA for vibration control

3.1. Objective structure

The target object for vibration control is a 3 mm-thick acrylic rectangular plate measuring 226 × 150 mm. The short side of the plate is fixed to form a cantilevered flat plate, suppressing the vibration in the out-of-plane direction. In addition, a finite element model for the target structure is created to perform a control simulation. Fig. 3 shows the mode shapes and the natural frequencies of the target object. The deformation and color mapping in Fig. 3 represent the mode shapes in the out-of-plane direction of the plate, where blue and red denote a small and large mode component, respectively. Table 1 shows the physical characteristics of the acrylic plate, which are tuned so that the calculated results of the natural frequencies fit the experimental values. It should be noted that the finite element analysis results in Fig. 3 exclude the 10th mode because its vibration is in the in-plane direction, which is beyond the scope of vibration control in this study.

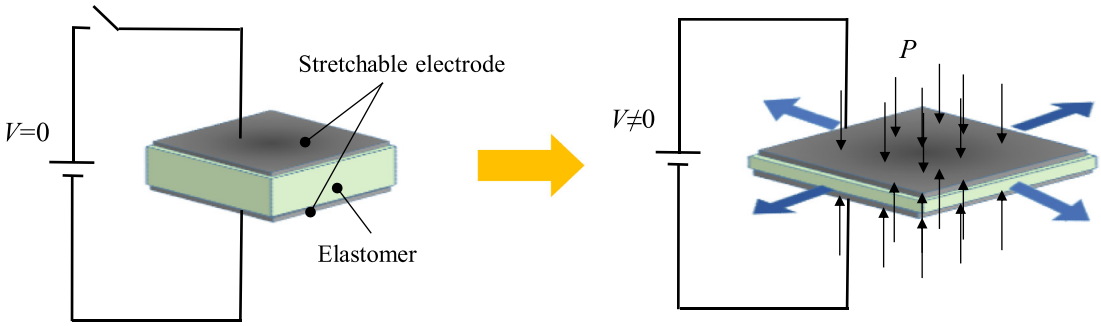

Fig. 1. Structure and actuation mechanism of DEA.

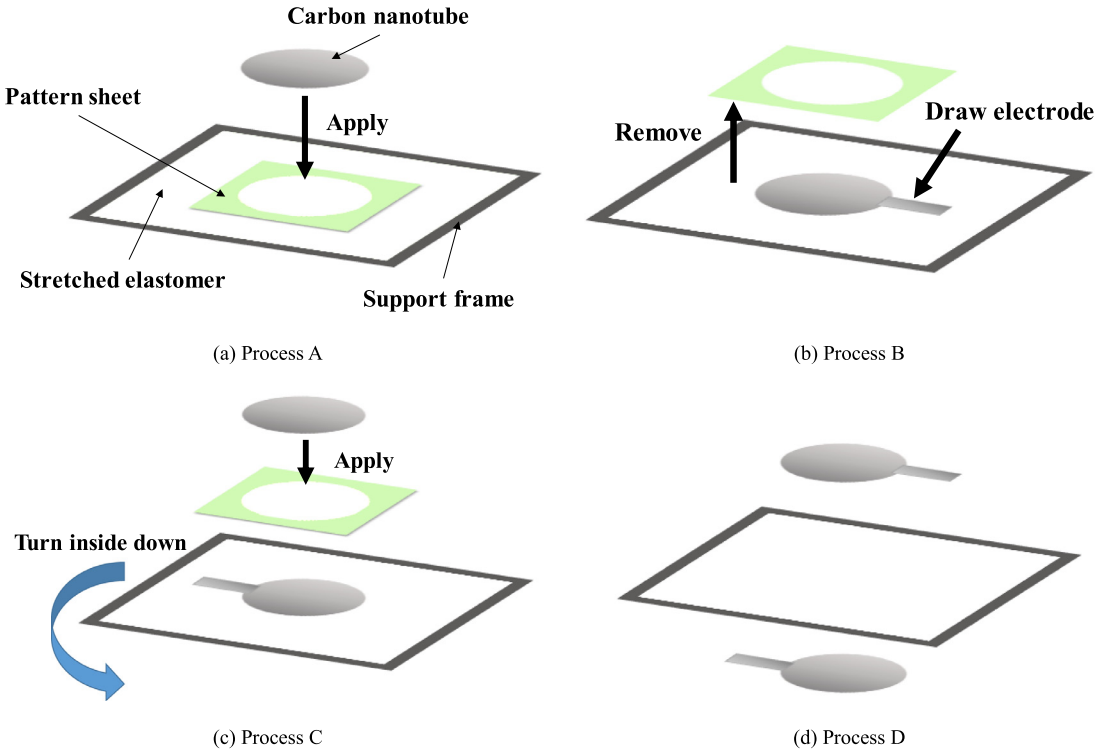

(a) Process A (b) Process B

(c) Process C (d) Process D

Fig. 2. Process to apply CNT to an elastomer.

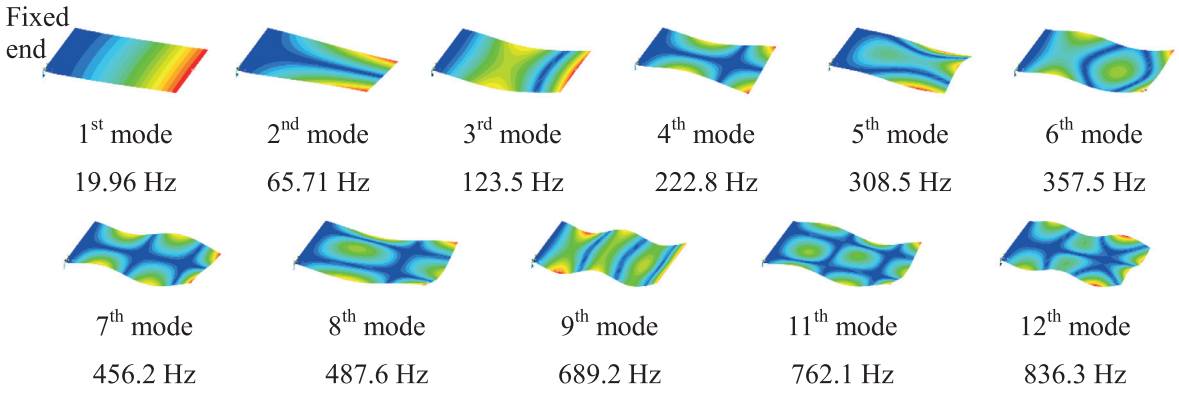

Fig. 3. Mode shapes obtained from FEA. (For interpretation of the references to color in this figure, the reader is referred to the web version of this article.)

Table 1
Parameters of the FE model of the target object.

Young's modules	4.5 GPa
Density	1100 kg/m^3
Poisson's ratio	0.35

3.2. Measurement system

To realize vibration control using the DEA, it should be confirmed that DEA excites the vibration of acrylic plates. The vibration measuring system is composed of an acrylic plate, an accelerometer (RION, PV-08A), a spectrum analyzer (A/D: ONO SOKKI, DS-2000, Software: CATEC, CAT-System), and a high output voltage amplifier (Trek, Model 609E-6, max voltage: ±4 kV) (Fig. 4). The DEA, which is prepared using the method discussed in Section 2, is attached to the acrylic plate. In this evaluation, the elastomer is affixed to the acrylic plate using only its sticky characteristic instead of using an adhesive. Details of the DEA's layer constitution are discussed in 3.3.

To determine the vibration characteristics of the acrylic plate, a swept sine wave is generated and inputted to the DEA via a voltage amplifier. The analysis frequency range is 1000 Hz and the number of sampling points is 4096. In addition, the amplitude of the voltage of the swept sine wave (V_{amp}) is changed appropriately within the range of 0.6–1.3 V, while the offset voltage with the same amplitude is set. Therefore, the output signal is the swept sine wave, where the offset voltage V_{amp} is the center voltage. The wave is amplified 1000 times via a high output voltage amplifier to ensure that the maximum voltage for DEA is between 1.2–2.6 kV.

3.3. DEA configuration

To evaluate the effective DEA layers in the vibration experiments, three kinds of configurations are discussed. Fig. 5 shows how the DEA is attached in each configuration. The lower part represents the acrylic plate. The dotted line represents a CNT and the flexible electrodes. The

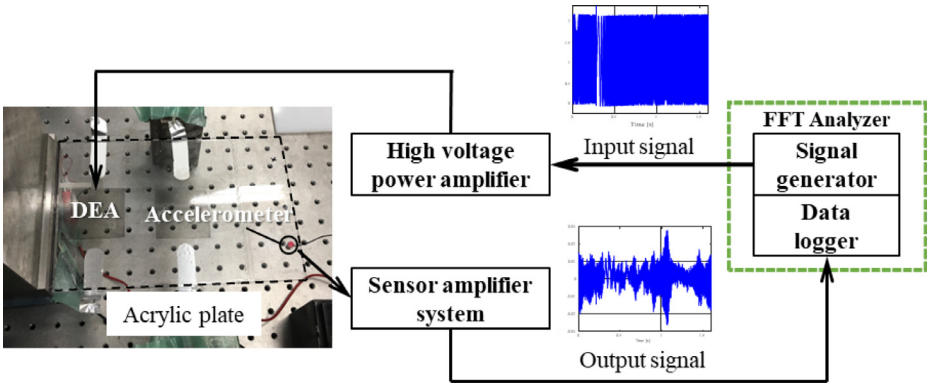

Fig. 4. Vibration measurement system.

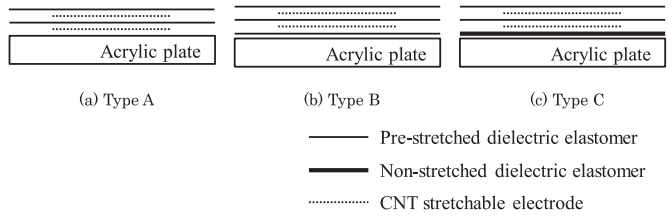

Fig. 5. DEA layers.

thin line denotes the elastomer with pre-stretching, while the bold line depicts the elastomer without pre-stretching.

Type A (Fig. 5(a)) does not excite the vibrations of the acrylic plate. It is possible that the force or moment generated by the DEA is not transmitted to the acrylic plate due to the lack of adhesive where the plate is covered by a CNT.

Type B has a pre-stretched elastomer between the layers of the acrylic plate and electrode (Fig. 5(b)). This configuration allows expansion of the DEA due to the shear strain in the additional bonding layer. Then another layer is added to the surface layer to prevent exposure of the CNT to air. The vibration measurement confirms that the acrylic plate vibrates, but structural breakdown inside the DEA occurs as the applied voltage increases.

As discussed above, the amount of generated stress increases with the applied voltage because the stress is proportional to the square of the voltage. However, if structural breakdown occurs, the generated stress decreases, degrading the actuator. Type C has a structure in which an elastomer layer without pre-stretching is added between the acrylic plate and the electrode surface (Fig. 5(c)). The elastomer without pre-stretching is about four times thicker (200 μm) than that with pre-stretching. Structural breakdown should be prevented by decreasing the stress induced in the DEA due to the additive layer without pre-stretching and making the additive layer thicker increases the applied moment to the acrylic plate.

To evaluate the excitation of the vibration of the DEA, a vibration measurement was conducted using Type B and Type C actuators. Fig. 6 depicts the experimental system. The upper DEA (U_{thin}) is Type B, while the lower DEA (U_{thick}) is Type C. Both DEAs measure 40 × 40 mm. U_{thin} and U_{thick} are attached to the acrylic plates symmetrically to the longitudinal centerline of the plates. Structural breakdown occurs in U_{thin} when a maximum voltage of 1.6 kV is applied. On the other hand, structural breakdown does not occur for U_{thick} even when the applied voltage is 2.6 kV. The layer composed of the elastomer without pre-stretching can conform to the large deformation of the electrode. Consequently, uneven strain does not occur inside the electrode.

Fig. 7 shows the Fourier spectrum of the vibration measurement. It should be noted that the averaging process involves 30 Fourier spectra in each DEA experiment. When considering the Fourier spectrum in Fig. 7 from the perspective of the stress generated by the DEA, the exciting force in U_{thick} is much larger than that in U_{thin}. Vibration excitations in the primary and the secondary modes are observed in U_{thick}, but not in U_{thin}. The increased thickness of the layer just below the electrode part extending in the in-plane direction may be responsible for the increased moment acting on the structure. Hence, the addition of an elastomer without pre-stretching allows the applied voltage to be increased, which, in turn, increases the exciting force and mode excitations. Based on these observations, the experiments below employ Type C DEA for vibration control.

3.4. Vibration control system

Fig. 8 shows the configuration of the vibration control system where U_{thick} is used as the control actuator. In this experiment, the external disturbance is an excitation by the PZT actuator. The PZT actuator, which

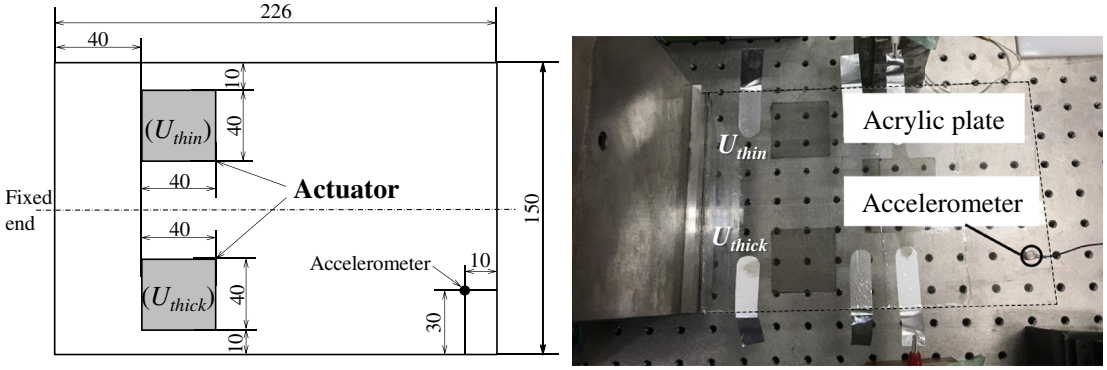

Fig. 6. Location of the two DEAs.

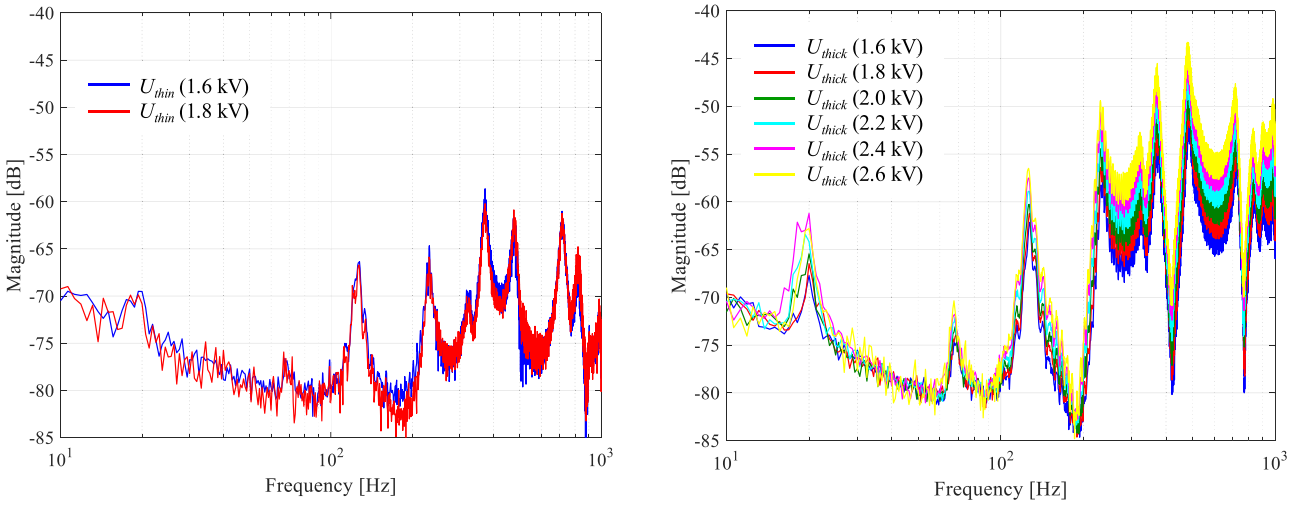

(a) Fourier spectrum with U_{thin}

(b) Fourier spectrum with U_{thick}

Fig. 7. Comparison of the Fourier spectra.

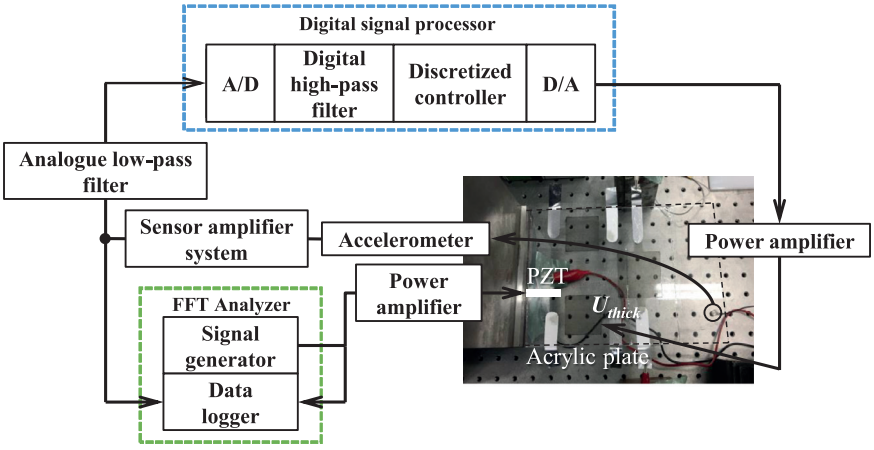

Fig. 8. Control system.

Table 2
Configuration of the vibration control system.

FFT analyzer	Product	ONO SOKKI, DS-2000
	Analysis frequency range	4 kHz
	Sampling points	4096
DSP	Product	Quanser, WinCon 5. 2
	Sampling frequency (f_s)	80 kHz
Analogue LPF	Product	NF Corporation, 3334
Digital HPF	–	(Built-in DSP)
Amp. (Sensor)	Product	ONO SOKKI, 2ch sensor amp. SR-2210
	Gain	×60
Amp. (PZT)	Product	NF Corporation, HSA4012
	Gain	×10
Amp. (DEA)	Product	Treck, Model 609E-6
	Gain	×1000
Accelerometer	Product	RION, PV-08A

measures 30 × 5 × 2 mm, is attached to the route area of the acrylic plate (Fig. 8). The voltage from a signal generator for the external disturbance is amplified tenfold, and the swept sine signals are inputted to the PZT actuator. An accelerometer is used to detect vibrations of the acrylic plate due to the external disturbance. The detected signal is inputted to a digital control system, and the DEA is operated using the control input calculated by the control system. Table 2 shows the specifications of the experimental system. These conditions are sufficient for active vibration control and frequency response analysis in the target frequency range.

4. Actuator location/shape and control system design

To achieve good control performance, the optimal arrangement and shape of the DEA are examined. An effective arrangement and shape of the actuator with respect to the intended vibration mode are critical

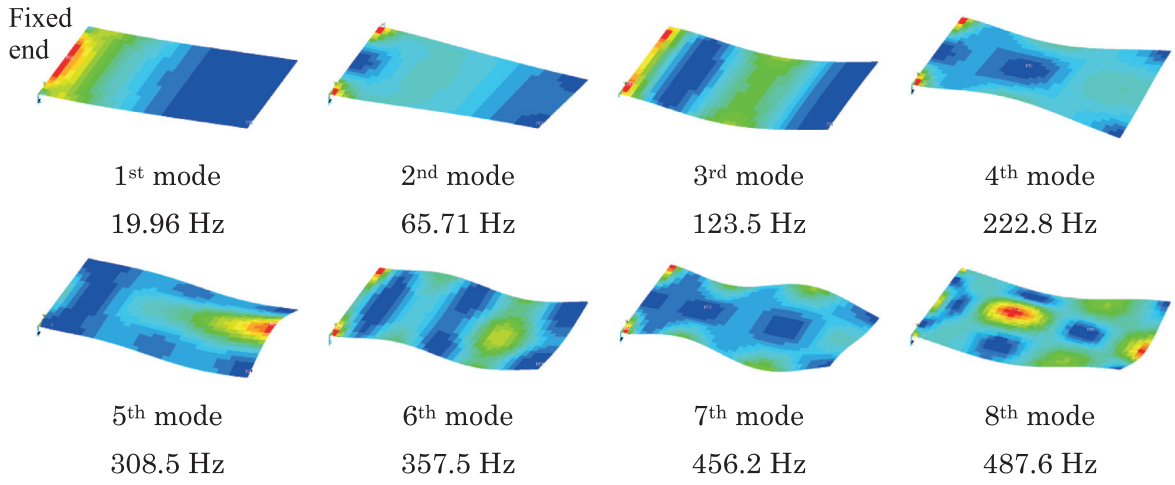

Fig. 9. Modal strain energy obtained from FEA. (For interpretation of the references to color in this figure, the reader is referred to the web version of this article.)

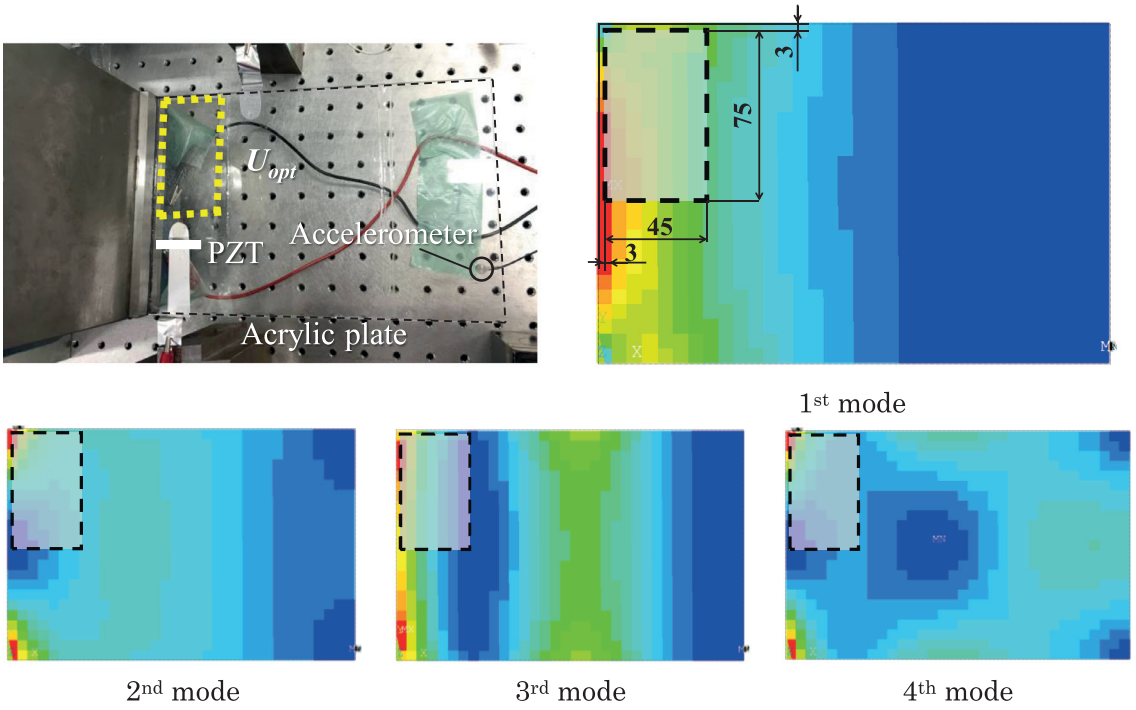

Fig. 10. Appropriate actuator location/shape due to the modal strain energy distribution.

to realize a stable and energy-efficient control system. The DEA adds an input moment to the structure because it extends in the in-plane direction on the surface of the structure. Hence, this study determines the arrangement and shape of the DEA to achieve effective control input by referring to the modal strain energy of the structure and derives the model to design the control system.

4.1. Modal strain energy and appropriate actuator location and shape

The modal strain energy is calculated based on tensile/compressive strain, shear strain, bending strain and torsional strain using the finite element method. Color mapping in Fig. 9 shows the distribution of the modal strain energy from the primary to the 8th modes, where blue and red denote a small and large strain energy, respectively. On the other hand, the deformation in Fig. 9 represents the mode shapes. This section discusses the effective arrangement and the shape of the DEA for the lower modes, namely the primary to the 4th modes.

The appropriate placement of the actuator is determined by the large contribution of the control input on the structure's response. In other words, the greater the difference in the strain of the structure at the ends of the actuator for the object mode to be controlled, the greater the contribution of the control input in the response of the structure for that mode. This means that when using a rectangular actuator, the difference between the distortion on the two opposing long sides and the strain on the two short sides is large with respect to the corresponding mode. Accordingly, the appropriate actuator location can be evaluated by observing the mode strain energy distribution of the structure. Considering the modal strain energy distribution in Fig. 9, Fig. 10 shows the arrangements and shapes of the actuator (Type C) that may provide a high vibration control performance for the primary to the 4th modes. The yellow dotted line (upper left) indicates the DEA. The rectangular DEA is fixed near the edge of the acrylic plate. The actuator location/shape is not symmetric with respect to the centerline of the plate in order to control both torsional and bending modes included in the control target modes. Fig. 10 shows that the difference in strain

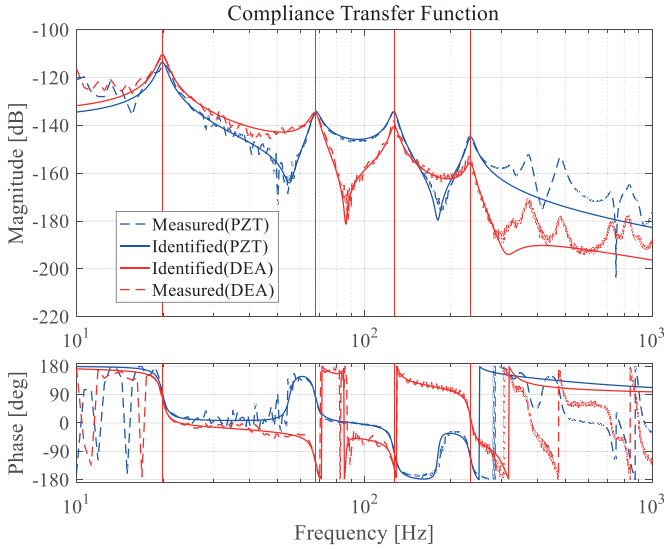

Fig. 11. System identification results.

Table 3
Identified modal parameters.

	1	2	3	4
ω_{dr} [Hz]	19.89	67.64	127.0	234.4
$\sigma_r \times 10^{-2}$	3.41	3.58	3.14	3.12

between the two opposing long sides and the two short sides is relatively large for all four corresponding modes with respect to the actuator location/shape. Consequently, the actuator location/shape shown in Fig. 10 is suitable for the vibration control of the four corresponding modes.

4.2. Modeling of the target object and control system design

Based on the experimental modal analysis, the open-loop system without a control is identified as the two-input one-output model. Accordingly, the state equation is derived. From the experimental modal analysis, the primary to the 4th modes are curve-fitted [29,32].

Fig. 11 shows the measured frequency responses and the resulting curve fittings for the frequency response function (FRF) to the external disturbance and control input. Table 3 lists the identified natural frequency (ω_{dr}) and the modal damping ratio (σ_r). The results shown in Fig. 11 confirm that the system identification is appropriate. It should be noted that the identified system, which is the open-loop system without a control, includes the passive damping effects due to the attached DEA.

Based on the modal parameters in Table 3, the control target system can be described as follows:

$$\dot{\boldsymbol{q}} = \boldsymbol{A}\boldsymbol{q} + \boldsymbol{B}_1\boldsymbol{w} + \boldsymbol{B}_2\boldsymbol{u} \tag{2}$$

$$\boldsymbol{y}_1 = \boldsymbol{C}_1\boldsymbol{q} + \boldsymbol{D}_{11}\boldsymbol{w} + \boldsymbol{D}_{12}\boldsymbol{u} \tag{3}$$

$$\boldsymbol{y}_2 = \boldsymbol{C}_2\boldsymbol{q} + \boldsymbol{D}_{21}\boldsymbol{w} + \boldsymbol{D}_{22}\boldsymbol{u} \tag{4}$$

Eq. (2) expresses the controlled object's state equation, where $\boldsymbol{q}$, $\boldsymbol{w}$, and $\boldsymbol{u}$ are the state vector, the external disturbance input vector, and the control input vector, respectively. $\boldsymbol{y}_1$ is the controlled variable vector, while $\boldsymbol{y}_2$ is the observed output vector. Each coefficient matrix ($\boldsymbol{A}$, $\boldsymbol{B}_1$, $\boldsymbol{B}_2$, $\boldsymbol{C}_1$, $\boldsymbol{C}_2$, $\boldsymbol{D}_{11}$, $\boldsymbol{D}_{12}$, $\boldsymbol{D}_{21}$, and $\boldsymbol{D}_{22}$) is defined by the identified modal parameters, the input conditions for the control input and the external disturbance, the physical quantity of the controlled variable, and the observed output. Details are described elsewhere [29,32]. In this modeling process, the controlled object is modeled as a linear system assuming that the deformation of the DEA is negligible, even though the DEA characteristics include some nonlinearities due to Maxwell stress, nonlinear elasticity, and viscoelasticity.

Table 4
Parameters for the weighting functions and filters.

Q		1.0×10^8	
R		1.0×10^4	
W_1		1	
W_2	Central frequency	HSF	2500 Hz
	Gain		40 dB
	Quality factor		0. 8
W_3		1	
Digital high-pass filter	Cut-off frequency	1 Hz	
	Order	1	
Analogue low-pass filter	Cut-off frequency	20 kHz	
	Order	4	

The controller design and control experiment are conducted to validate the DEA configuration obtained in 3.3 and the DEA location/shape obtained in 4.1. The controller is designed based on the H_∞ control theory. Fig. 12(a) shows the block diagram of the control system. Here, $\boldsymbol{G}(s)$ is the generalized controlled object in the output feedback system, and $\boldsymbol{K}(s)$ is the controller. Fig. 12(b) shows the configuration of the generalized controlled object $\boldsymbol{G}(s)$, whereas $\boldsymbol{Q}$ and $\boldsymbol{R}$ are weighting matrices for the controlled response ($\boldsymbol{z}_1$) and the control input ($\boldsymbol{u}$), respectively. $\boldsymbol{W}_1$ and $\boldsymbol{W}_2$, which are used for frequency shaping, are the frequency weighting functions for the controlled response and the control input, respectively. $\boldsymbol{W}_2$ focuses the control on the objective modes, which are the damping targets under the constraint of a robust stability for the high order vibrations by applying frequency shaping of the control input. $\boldsymbol{W}_3$ is the frequency weighting function for the observed output corresponding to the output filter. The controller is designed based on the H_∞ control problem (5), which minimizes the H_∞ norm of the transfer function matrix from the external disturbance ($\boldsymbol{w}$) to the controlled variable ($\boldsymbol{y}_1$).

$$\mathbf{min}\,.\|\boldsymbol{T}_{\boldsymbol{y1w}}\|_\infty \tag{5}$$

The H_∞ control is applied to achieve the worst case vibration suppression and the control input limitation due to the evaluation based on the H_∞ norm of the transfer function matrix $\boldsymbol{T}_{y1w}$. The control system design is conducted using the Control System Toolbox from MATLAB.

In the control problem, the acceleration responses are used as the controlled response and the observed output. Additionally, a high-shelf filter with a center frequency of 2500 Hz is used as the frequency weighting function (W_2). Table 4 shows the other parameters used to design the controller. These parameters are selected to realize sufficient vibration suppression.

5. Results and discussion

Fig. 13 shows the frequency response of the displacement versus the input of the external disturbances from the vibration control simulation. Within the frequency band that includes all of the identified modes, effective vibration control is achieved. At each resonance peak, vibration suppression effects of 10–15 dB are confirmed.

Next, using the system described in Fig. 10, Tables 2 and 4, a control experiment was conducted. Fig. 14 shows the frequency response of the acceleration response to an external disturbance. The first four modes have reduced vibrations of –10.5 dB, –7.7 dB, –11.6 dB, and –7.9 dB, respectively. Each mode shows a great vibration suppression effect. Additionally, the results of the control experiment are similar to the simulation results, demonstrating the efficacy of the DEA for vibration control.

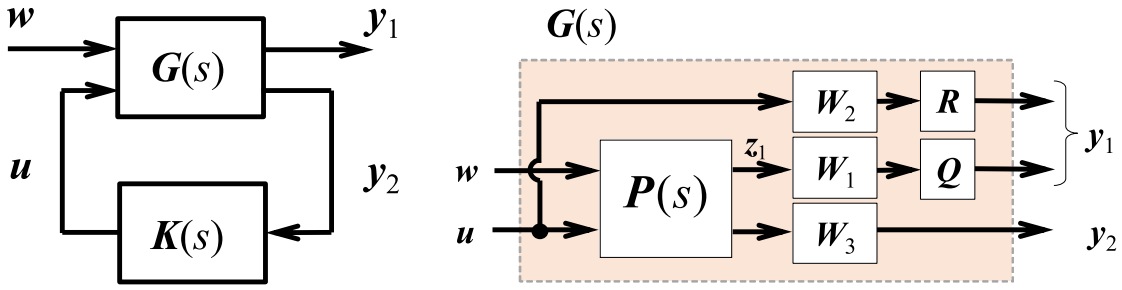

(a) Block diagram of the closed-loop control system

(b) Details of the generalized plant of the controlled object

Fig. 12. Block diagram of the control system.

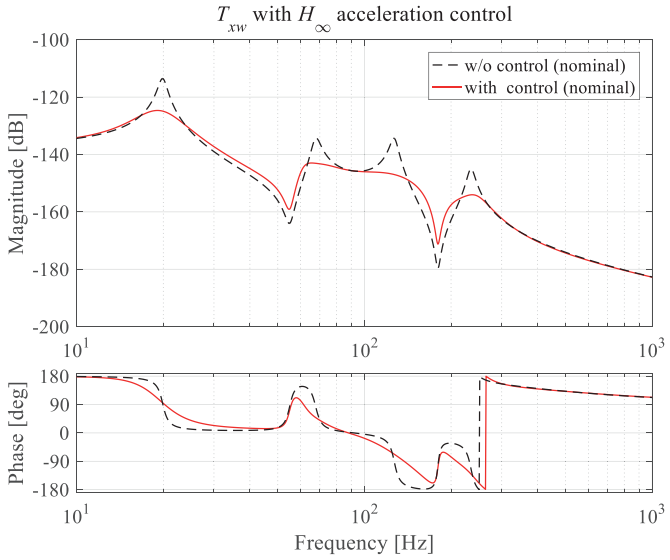

Fig. 13. Calculated closed-loop FRF of the displacement response.

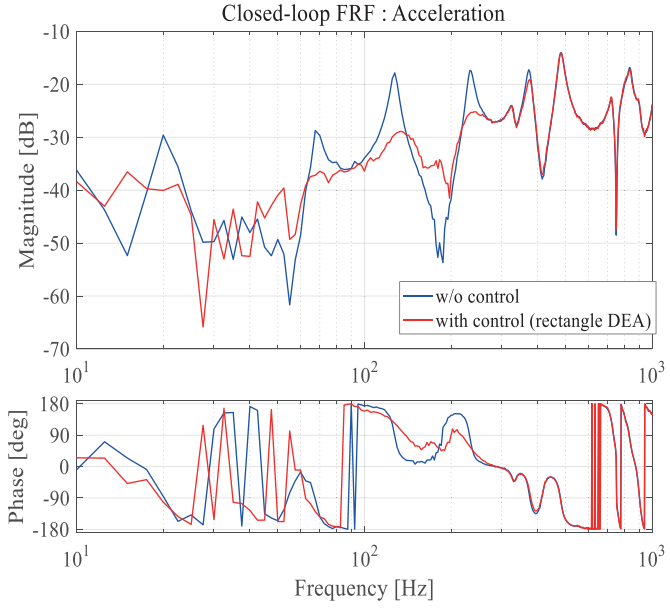

Fig. 14. Measured closed-loop FRF of the acceleration in the control experiment.

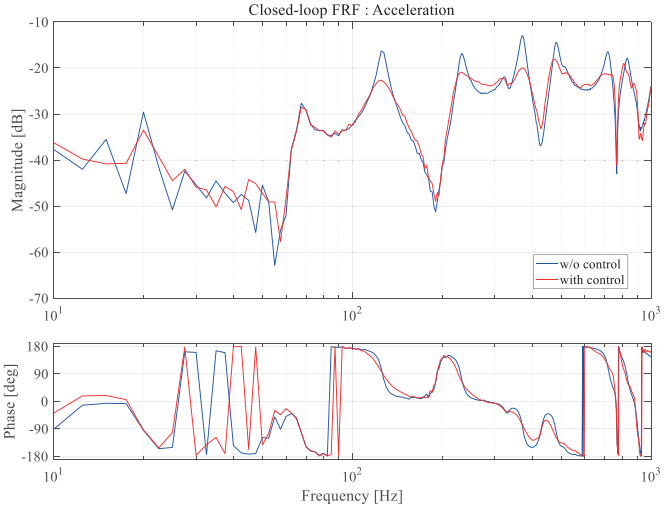

Fig. 15. Measured closed-loop FRF with 'thick' DEA in Fig. 6.

For comparison, Fig. 15 shows the results of the control experiment (acceleration FRF) using a 'thick' DEA (Fig. 6) without an optimized arrangement or shape. The configuration is identical to the optimized one except for the arrangement and the shape. For the control design parameters: $Q = 1.0 \times 10^{11}$ and $R = 1.0 \times 10^{6}$. All other parameters are the same as those shown in Table 4. The weighting matrices, $\boldsymbol{Q}$ and $\boldsymbol{R}$, are tuned to maximize vibration suppression in this condition. The non-optimized actuator has reduced resonance responses in most modes included within the controlled frequency band.

Compared to the optimized system (Fig. 14), the non-optimized system shows smaller vibration suppression effects, especially in the lower modes. This difference is attributed to the arrangement and the shape of the 'thick' DEA (Fig. 6) because the actuator does not effectively contribute to certain modes. These results demonstrate that the arrangement and the shape of the actuator must be determined with respect to the strain energy.

6. Conclusions

This study examined vibration control using the DEA. First, the driving mechanism and the manufacturing method of DEAs were presented. Then the vibration characteristics of an acrylic plate as a controlled object when the DEA is used as a driving actuator were evaluated. To achieve effective vibration excitation, different patterns of DEA layers were tested to identify the configuration where structural breakdown does not occur and a greater force is generated. Next, the arrangement and shape of the DEA were investigated to effectively and efficiently

apply the force generated by the DEA to the controlled object, with a focus on the strain energy on the structure. A control simulation and an experiment on the optimized system confirmed that effective vibration suppression is achieved in the intended modes. Finally, the optimized actuator was compared to other actuators with different arrangements and shapes. In this manner, the efficacy of the vibration suppression method proposed by this study was verified. In the future, we plan to apply a DEA for vibration control of a curved surface.

Acknowledgments

We thank the Japan Society for the Promotion of Science for their support under Grants-in-Aid for Scientific Research Programs (Grants-in-Aid for Scientific Research (B), Project nos. JP16H04286, JP16H04291 and JP16H04306, and Grants-in-Aid for Challenging Exploratory Research, Project nos. JP17K18858 and JP16K14201).

References

[1] Pelrine RE, Kornbluh RD, Joseph JP. Electrostriction of polymer dielectrics with compliant electrodes as a means of actuation. Sens Actuator A 1998;64:77–85.
[2] Foo CC, Cai S, Koh SJA, Bauer S, Suo Z. Model of dissipative dielectric elastomers. J Appl Phys 2012;111:034102.
[3] Willser M, Mazza E. Electromechanical coupling in dielectric elastomer actuators. Sens Actuator A 2007;138:384–93.
[4] Kovacs G, During L, Michel S, Terrasi S. Stacked dielectric elastomer actuator for tensile force transmission. Sens Actuator A 2009;155:299–307.
[5] Shigemune H, Sugano S, Nishitani J, Yamauchi M, Hosoya N, Hashimoto S, Maeda S. Dielectric elastomer actuators with carbon nanotube electrodes painted with a soft brush. Actuators 2018;7:51.
[6] Hosoya N, Baba S, Maeda S. Hemispherical breathing mode speaker using a dielectric elastomer actuator. J Acoust Soc Am 2015;138(, 4):EL424–8.
[7] Hosoya N, Masuda H, Maeda S. Balloon dielectric elastomer actuator speaker. Appl Acoust 2019;148:238–45.
[8] Pelrine R, Kornbluh R, Pei Q, Joseph J. High-speed electrically actuated elastomers with strain greater than 100%. Science 2000;287:836–9.
[9] Loverich JJ, Kanno I, Kotera H. Concepts for a new class of all-polymer micropumps. Lab Chip 2006;6:1147–54.
[10] Chiba S, Wakib M, Kornbluha R, Pelrine R. Innovative wave power generation system using electroactive polymer artificial muscles. Proc IEEE Ocean 2009:1–3.
[11] Heydt R, Pelrine R, Joseph J, Eckerle J, Kornbluh R. Acoustical performance of an electrostrictive polymer film loudspeaker. J Acoust Soc Am 2000;107:833–9.
[12] Heydt R, Kornbluh R, Eckerle J, Pelrine R. Sound radiation properties of dielectric elastomer electroactive polymer loudspeakers. In: Proceedings of the SPIE smart structures and materials conference, 6168; 2006. p. 64–6188.
[13] Sugimoto T, Ono K, Ando A, Morita Y, Hosoda K, Ishii D. Semicylindrical acoustic transducer from a dielectric elastomer film with compliant electrodes. J Acoust Soc Am 2011;130:744–52.
[14] Sugimoto T, Ando A, Ono K, Morita Y, Hosoda K, Ishii D, Nakamura K. A lightweight push-pull acoustic transducer composed of a pair of dielectric elastomer films. J Acoust Soc Am 2013;134:EL432–7.
[15] Akbari S, Rosset S, Shea HR. Improved electromechanical behavior in castable dielectric elastomer actuators. Appl Phys Lett 2013;102:071906.
[16] Poulin A, Rosset S, Shea HR. Printing low-voltage dielectric elastomer actuators. Appl Phys Lett 2015;107:244104.
[17] Ji X, Rosset S, Shea HR. Soft tunable diffractive optics with multifunctional transparent electrodes enabling integrated actuation. Appl Phys Lett 2016;109:191901.
[18] Lau G-K, Heng K-R, Ahmed AS, Shrestha M. Dielectric elastomer fingers for versatile grasping and nimble pinching. Appl Phys Lett 2017;110:182906.
[19] Minaminosono A, Shigemune H, Okuno Y, Katsumayta T, Hosoya N, Maeda S. Deformable motor driven by dielectric elastomer actuators and flexible mechanisms. Front Robot AI 2019;6:1.
[20] Papaspiridis F-G, Antoniadis I-A. Dielectric elastomer actuators as elements of active vibration control systems. Adv Sci Technol 2008;61:103–11.
[21] Sarban R, Jones R-W, Mace B-R, Rustighi E. A tubular dielectric elastomer actuator: fabrication, characterization and active vibration isolation. Mech Syst Signal Process 2011;25:2879–91.
[22] Sarban R, Jones R-W. Physical model-based active vibration control using a dielectric elastomer actuator. J Intell Mater Syst Struct 2012;23:473–83.
[23] Berselli G, Vertechy R, Babic M, Castelli V-P. Dynamic modeling and experimental evaluation of a constant-force dielectric elastomer actuator. J Intell Mater Syst Struct 2012;24:779–91.
[24] Karsten R, Lotz P, Schlaak H-F. Active suspension with multilayer dielectric elastomer actuator. In: Proceedings of the SPIE smart structures and materials + nondestructive evaluation and health monitoring, 7976; 2011. doi:10.1117/12.880459.
[25] Nishidome C, Kajiwara I. Motion and vibration control of flexible-link mechanism with smart structure. JSME Int J Ser C 2003;46:565–71.
[26] Ohashi F, Kajiwara I, Iwadare M, Arisaka T. Optimal design of smart carriage arm in magnetic disk drive for vibration suppression. Microsyst Technol 2005;11:711–17.
[27] Ono K, Kajiwara I, Ishizuka S. Piezoelectric and control optimization of smart structures for vibration and sound suppression. Int J Veh Des 2007;43:184–99.
[28] Honda S, Kajiwara I, Narita Y. Multidisciplinary design optimization for vibration control of smart laminated composite structures. J Int Mater Syst Struct 2011;22:1419–30.
[29] Kajiwara I, Furuya K, Ishizuka S. Experimental verification of real-time tuning method of a model-based controller by perturbations to its poles. Mech Syst Signal Process 2018;107:396–408.
[30] Shintake J, Cacucciolo V, Shea HR, Floreano D. Soft biomimetic fish robot made of dielectric elastomer actuators. Soft Robot 2018;5:466–74.
[31] Shintake J, Cacucciolo V, Shea HR. Soft robotic grippers. Adv Mater 2018;30:1707035.
[32] Zhang Y, Hiruta T, Kajiwara I, Hosoya N. Active vibration suppression of membrane structures and evaluation with a non-contact laser excitation vibration test. J Vib Control 2017;23:1681–92.